Late Eemian warming in the Nordic Seas as seen in proxy data and climate models

A. Born[1,2], K. H. Nisancioglu[1], B. Risebrobakken[1], A. Levermann[3,4]

A. Born, Allégaten 55, 5007 Bergen, Norway. (andreas.born@bjerknes.uib.no)

[1]Bjerknes Centre for Climate Research, Bergen, Norway

[2]Geophysical Institute, University of Bergen, Bergen, Norway

[3]Potsdam Institute for Climate Impact Research, Potsdam, Germany

[4]University of Potsdam, Institute of Physics, Potsdam, Germany

We analyze a transient simulation of the last glacial inception in a climate model of intermediate complexity, focusing on sea ice-ocean circulation dynamics in the North Atlantic and Nordic Seas. This expands work previously done with time slice simulations from a high resolution model and provides important clues for the interpretation of climate proxy data from the last glacial inception. As northern high latitude summer insolation decreases towards the end of the Eemian interglacial, Arctic sea ice export to the North Atlantic increases. This surface fresh water transport weakens deep water formation in the North Atlantic and the surface circulation of the subpolar gyre. As a consequence, the relative contribution of subpolar gyre waters to the Atlantic inflow into the Nordic Seas is reduced, giving way to more warm and saline subtropical waters from the North Atlantic Current. We thus find an episode of relatively high heat and salt transport into the Nordic Seas during the last glacial inception between 118,000 and 114,000 years before present. This stabilizes deep ocean convection in the region and warms Scandinavia during the phase of lowest insolation. These findings are in good agreement with proxy data from the Nordic Seas and North Atlantic. At the end of the warm interval, sea surface temperature drops by about 3°C, probably marking the onset of large scale glacier growth over Scandinavia.

1. Introduction

The last glacial inception about 115,000 years ago (115 ka) was a period of exceptionally low summer insolation in northern high latitudes. This facilitated the nucleation of continental scale ice sheets in the Northern Hemisphere and triggered feedback processes which eventually led to the end of the interglacial climate and a shift to a cold glacial climate [*de Noblet et al.*, 1996; *Khodri et al.*, 2001; *Calov et al.*, 2005].

There is, however, evidence that the cooling due to lower insolation was not homogeneous and that relatively high temperatures prevailed in the eastern North Atlantic [*Chapman and Shackleton*, 1999; *Bauch and Kandiano*, 2007] and the eastern and northern Nordic Seas [*Risebrobakken et al.*, 2007] throughout the insolation minimum. The warming is attributed to a strengthening of the Norwegian Atlantic Current (NwAC), carrying warm and saline water from the Atlantic Ocean through the Nordic Seas into the Barents Sea and Arctic Ocean (Fig. 1). It plays an important role in the formation of deep waters and changes in its strength likely impact the deep outflow from the Nordic Seas. A weakening of this deep current only after the insolation minimum also suggests that the NwAC continued to be active [*Rasmussen et al.*, 1999]. Further south, in the central North Atlantic, a northward shift of the North Atlantic Current is reported coeval with the strengthening of the NwAC [*Cortijo et al.*, 1999]. The combined evidence from proxy data thus indicates a reorganization of the large scale current system.

Previous modeling work identified the following chain of events in the coupled climate model IPSL CM4 [*Born et al.*, 2010]: decreased summer insolation in northern high latitudes at 115 ka compared to 126 ka increases the Arctic sea ice volume. Thus, thicker

sea ice is transported southward in the East Greenland Current, freshening the surface waters of the North Atlantic. Consequently, deep convection is shut down in this region and the altered density structure weakens the subpolar gyre. This in turn reduces the relative contribution of the subpolar gyre to a water mass formed in the Rockall region of the eastern North Atlantic, giving way to more warm and saline subtropical waters to enter the Nordic Seas [*Hátún et al.*, 2005]. This mechanism counteracts decreasing insolation and the general freshening trend due to enhanced sea ice transport (Fig. 2). The weaker subpolar gyre also allows for a northward shift of the North Atlantic Current, observed as a warm anomaly and a salinity dipole off Newfoundland.

In the present study we expand this work with a transient simulation. The aim is to investigate if findings from proxy data can be reproduced in a physically consistent climate model and thus provide a detailed description of the regional climate evolution of the last glacial inception. The North Atlantic surface circulation is found to play an important role. Following a description of models in Section 2 and proxy data in Section 3, results of the two coupled climate models are analyzed in Section 4. Based on the model results, an interpretation and discussion of proxy data is given in Section 5. We summarize and conclude in Section 6.

2. Model Description and Experiments

This study combines simulations of a high resolution ocean atmosphere general circulation model, IPSL CM4 [*Marti et al.*, 2009], and a coupled climate model of intermediate complexity CLIM*BER*-3α [*Montoya et al.*, 2005]. Time slice experiments have been carried out for 126 ka and 115 ka in both models, and integrated to quasi-equilibrium. In

addition, a transient simulation with CLIM*BER*-3α was integrated from the end of the 126 ka equilibrium with variable orbital forcing through to the year 110 ka.

All experiments are forced by orbital insolation following *Berger* [1978] and fixed greenhouse gas concentrations at the preindustrial level (CO_2, 280 ppmv). The latter is a good approximation for the Eemian and the last glacial inception until about 112 ka [*Petit et al.*, 1999]. After that, CO_2 concentration decreased gradually to 250 ppmv at 110 ka. This is not included in the simulations. Details of the models and relevant references are given below.

2.1. IPSL

The Institut Pierre Simon Laplace coupled model version 4 (IPSL CM4) comprises ocean, sea ice, atmosphere and land surface components. The ocean model's dynamical core is based on the OPA system [*Madec et al.*, 1997]. The configuration used here (ORCA2) uses a horizontal resolution based on a 2 degree Mercator mesh, enhanced to 0.5 degree meridional resolution near the equator for a better representation of the equatorial wave channel and with two poles over the continents in the Northern Hemisphere in order to avoid a singularity in the Arctic Ocean. There are 31 unevenly spaced levels in the vertical. A free surface formulation is used for the upper boundary [*Roullet and Madec*, 2000], and a diffusive boundary parametrization is used for the bottom [*Beckmann*, 1998].

The dynamic sea ice model (LIM2, *Fichefet and Maqueda* [1997, 1999]) uses the horizontal ocean grid to compute ice rheology and advection. Thermodynamics are computed in three vertical layers, the uppermost for snow. Ice growth and melting are determined by an energy balance at both the snow-ice- and water boundary and in leads. Internal

forces follow a viscous-plastic law [*Hibler*, 1979]. The model features parametrizations for the trapping of shortwave radiation by brine pockets, leads in the ice, as well as an implicit representation of subgrid variations in snow and ice thickness.

The atmosphere is modeled by a comprehensive general circulation model (LMDZ, *Hourdin et al.* [2006]) with a resolution of 3.75 zonally and 2.5 meridionally on 19 vertical levels. Precipitation over land is returned to the ocean by means of a river routing scheme implemented in the land surface model (ORCHIDEE, *Krinner et al.* [2005]).

The simulations for 126 ka and 115 ka were initiated with an ocean at rest and preindustrial hydrography [*Levitus*, 1982] and integrated for 300 and 800 years, respectively. The results presented are calculated from averages over the last 100 years of the simulations. More information on the simulations can be found in *Braconnot et al.* [2008] and *Born et al.* [2010].

2.2. CLIM*BER*-3α

CLIM*BER*-3α consists of the statistical-dynamical atmospheric model POTSDAM-2 [*Petoukhov et al.*, 2000] coupled to a global, 24-layer ocean general circulation model based on the Geophysical Fluid Dynamics Laboratory (GFDL) Modular Ocean Model version 3 (MOM-3) code and to the dynamic and thermodynamic sea ice module of *Fichefet and Maqueda* [1997]. The oceanic horizontal resolution is $3.75^\circ \times 3.75^\circ$. We apply a weak background vertical diffusivity of 0.2×10^{-4} m^2/s. For a discussion of the model's sensitivity to this parameter refer to *Mignot et al.* [2006]. Sea ice albedo is increased by 5% compared to *Montoya et al.* [2005] in order to ensure a more realistic Arctic sea ice cover at 126 ka. This small change is within uncertainties of observed ice albedo values.

The atmospheric model has a coarse spatial resolution (7.5° in latitude and 22.5° in longitude) and is based on the assumption of a universal vertical structure of temperature and humidity, which allows reducing the three-dimensional description to a set of two-dimensional prognostic equations. Heat and freshwater fluxes between the ocean and the atmosphere are computed on the oceanic grid and applied without any flux adjustments. The wind stress is computed as the sum of the NCEP-NCAR reanalysis wind stress climatology [*Kalnay and coauthors*, 1996] and the wind stress anomaly calculated by the atmospheric model relative to a preindustrial control run.

This model has been used in several studies of past climates [*Montoya et al.*, 2010; *Born and Levermann*, 2010] and future projections [*Gregory et al.*, 2005; *Stouffer et al.*, 2006].

Time slice experiments for 126 ka and 115 ka were initialized from the preindustrial control experiment and run to equilibrium for more than 2000 years. In order to reduce the high computational cost of the transient simulation, the orbital forcing is accelerated by a factor of three. Thus, the simulated 16,000 years from 126 ka to 110 ka correspond to about 5400 model years. Atmospheric chemical composition, land surface topography and albedo were fixed and thus neglect feedbacks of the progressing glacial inception. However, as discussed in Section 4, findings presented here should not depend critically on this simplification. A control experiment with forcing fixed at 126 ka was run in parallel.

3. Marine sediment cores and proxy data

Marine proxy records from cores MD99-2304 (eastern Fram Strait), MD95-2010 (Vøring Plateau) and NEAP18K (Rockall Plateau) are presented (Fig. 1). The cores are located

along the pathway of Atlantic water towards the Arctic. From MD99-2304 and MD95-2010 relative abundances of *Neogloboquadrina pachyderma* (sin) and *Neogloboquadrina pachyderma* (dex) are shown, as well as calculated SSTs. Planktic $\delta^{18}O$ of *Globigerina bulloides* and transfer function based SSTs are shown from NEAP18K. All records, except from the SSTs of MD99-2304 and MD95-2010, are previously published. Detailed information on methods and establishment of chronologies can be found in the original publications (Tab. 1). The chronology of NEAP18K is taken from *Chapman and Shackleton* [1999]. The summer SSTs of MD99-2304 and MD95-2010 have been calculated based on the relative abundances of *N. pachyderma* (sin) ($T = -0.07 \cdot (\%N.\ pachyderma(sin)) + 12.5$) [*Johannessen*, 1987]. This SST equation is restricted by an upper and lower temperature limit of 5.5°C and 12.4°C, respectively. The amplitude of our SST estimates may be affected, most probably by providing to warm temperatures in the cold end.

4. Model Results

While resolution is significantly lower in CLIM*BER*-3α compared to IPSL CM4, the key elements determining the dynamical changes depend on large scale features of the climate system and are thus well reproduced (Fig. 3). The much shorter integration after initialization with preindustrial data in IPSL CM4 is not critical either, probably because the previous interglacial was relatively similar to preindustrial climate. At 126 ka, most of the Arctic winter sea ice is thinner than 3 m in IPSL CM4, and thinner than 2 m in CLIM*BER*-3α. Both models simulate a similar area of winter sea ice exceeding 5 m thickness at 115 ka. Sea ice volume transport through Denmark Strait increases in both models, by 53 mSv in IPSL CM4 and 23 mSv in CLIM*BER*-3α (1 Sv = 10^6 m^3/s). The

subpolar gyre weakens from 26 Sv to 18 Sv between 126 ka and 115 ka in IPSL CM4 and from 29 Sv to 19 Sv in CLIM*BER*-3α.

Analysis of the transient experiment supports the following causal chain led by changes in summer insolation (Fig. 4). Arctic sea ice export through Denmark Strait increases as summer insolation decreases. The associated freshwater transport weakens the subpolar gyre first gradually and after 118 ka in a rapid transition. Concurrently, northward heat transport by the NwAC increases by $\sim 39 \cdot 10^{12}$ W (16 %). As summer insolation increases again the process is reversed with a second abrupt transition at 114 ka. This is in good agreement with the relative warming and salinification of the NwAC found in IPSL CM4 (Fig. 2). Note that despite increased heat transport by the NwAC no absolute warming is expected at 115 ka because of the counteracting large insolation forcing (Fig. 4a). Similarly, enhanced salt transport counteracts the general freshening by sea ice locally but does not reverse it. However, this is enough to stabilize deep water formation in the Nordic Seas (Fig. 4e) [*Born et al.*, 2010].

Although not directly comparable, fluxes in CLIM*BER*-3α are generally similar to present-day observations by *Hansen and Østerhus* [2000]: about 7 Sv of Atlantic water and 0.25 PW of heat enter the Nordic Seas as a surface current between Iceland and Scotland. This is approximately the same section used for the model in figure 4d. Observed sinking in the Nordic Seas is about 6 Sv.

Stabilization of Nordic Seas deep water formation is also seen in mixed layer depth (Fig. 5). Deep convection remains active in the Nordic Seas despite the general freshening and more extent sea ice (Fig. 2). Absolute values differ between the two models. Although,

not directly comparable, the IPSL CM4 simulates a shallower mixed layer at 115Ka than CLIMBER3a. It is possible that the high resolution IPSL CM4 model requires a longer integration time to equilibrate the deep ocean with a possible impact on the formation of deep water. At the same time, a long known deficiency of coarse resolution models is the imperfect representation of the southward outflow from the Nordic Seas over the deep and narrow sills of the Greenland Scotland ridge [*Roberts and Wood*, 1997; *Thorpe et al.*, 2004; *Born et al.*, 2009]. As a result bottom waters leaving the Nordic Seas are less dense than observed and the reservoir of deep dense water in the Nordic Seas is not optimally represented which again changes deep convection. The main conclusion, however, a stable deep circulation in the Nordic Seas at 115 ka, is consistent with both models. South of the Greenland Scotland ridge, IPSL CM4 shows two deep convection regions of which only one is active at 115 ka. CLIM*BER*-3α does not resolve two distinct regions but does simulate weaker convection at 115 ka. This is a result of weaker salt advection in the subpolar gyre in both models [*Levermann and Born*, 2007; *Born et al.*, 2010].

Note that the climate evolution is underestimated towards the last part of our simulations, due to neglecting transient climate forcings such as changes in atmospheric greenhouse gasses, land ice and vegetation. A reduction in atmospheric CO_2 started at approximately 112 ka [*Petit et al.*, 1999] and reached a value 30 ppm below the interglacial average at 110 ka, about one third of the full glacial-interglacial difference. Global eustatic sea level declined $\sim$40m between 120 ka and 110 ka due to the accumulation of ice on land [*Waelbroeck et al.*, 2002]. Considering these long term changes, the last part of

the transient simulation has to be interpreted carefully. The abrupt transition described here, however, occurred before the large changes in CO_2 and sea level.

5. Evidence of strong Norwegian Atlantic Current from Proxy Data

Our model experiments compare well to a number of marine proxy records throughout the North Atlantic and Nordic Seas (Fig. 1 and Tab. 1). The simulation shows that maximum heat transport by the NwAC occurs around the time of minimum northern high latitude summer insolation, lasting from 118 ka until 114 ka, in good agreement with foraminiferal faunal data from the Vøring Plateau (MD95-2010, Fig. 6a) and the slope of western Spitsbergen (MD95-2304, Fig. 6b) [*Risebrobakken et al.*, 2007]. Relatively high occurrence of the subpolar species *N. pachyderma* (dex) and Turborotalita quinqueloba (data not shown) and low levels of the polar species *N. pachyderma* (sin) mark the peak of the interglacial warmth in both cores between approximately 126 ka and 120 ka. As insolation decreases, the relative abundance of *N. pachyderma* (sin) increases until 118 ka, when the trend reverses. The interval between 118 ka and 114 ka represents a partial recurrence of the subpolar species and thus interglacial conditions in both cores. By reconstructing surface temperature from the relative abundance of *N. pachyderma* (sin) [*Johannessen*, 1987], the temperature drop after the transient warm phase is estimated to about 3°C on the Vøring Plateau and 1.2°C off western Spitsbergen. The late Eemian warming is also seen in other cores from the Norwegian Sea, and it has been argued for an Eemian climatic optimum, with the most intense advection of Atlantic surface water 118.5 ka - 116 ka [*Bauch and Erlenkeuser*, 2008].

A warm pulse is also found on the Rockall Plateau (NEAP18K) at about 115 ka, both in transfer function SST estimates based on foraminiferal assemblages and planktic $\delta^{18}O$ in the surface dwelling species *Globigerina bulloides* (Fig. 6c) [*Chapman and Shackleton*, 1999]. These findings are supported by similar results seen in M23414 [*Bauch and Kandiano*, 2007]. This North Atlantic warmth supports the hypothesis that the warm pulse in the Nordic Seas originates in the North Atlantic and that the warm pulse is related to increased meridional heat transport across the Greenland Scotland ridge.

The detailed time slice simulations show surface warming off Newfoundland in the central North Atlantic (Fig. 2, upper). As explained above, this is the result of a weaker subpolar gyre and a subsequent northward shift of the North Atlantic Current, providing additional means to test the dynamical hypothesis of this study with proxy data. Warmer and more saline water is seen during the late interglacial in the central North Atlantic (Fig. 1, CH69-K9 and SU90-03), in reconstructions based on planktic $\delta^{18}O$ [*Cortijo et al.*, 1999]. Generally, the prolonged warmth of the last interglacial, beyond the insolation minimum, is well documented for the eastern subpolar North Atlantic [*Ruddiman and McIntyre*, 1975; *McManus et al.*, 2002].

In addition to the surface proxy data, evidence exists for a stable deep outflow from the Nordic Seas until 114 ka (MD95-2009, [*Rasmussen et al.*, 1999]). This outflow is fed by downwelling water masses in the Nordic Seas and thus corroborates the model simulation of an active deep circulation in the Nordic Seas (Fig. 4e). The single marine sediment core, however, represents only one branch of the deep outflow and can not constrain the absolute change of the deep outflows.

Warming towards the end of the Eemian interglacial can also be found in terrestrial data from southern Norway at Fjøsanger, indicated by the appearance of Ilex pollen (holly) [*Mangerud et al.*, 1981]. Thus, there is consistence also between our marine data and terrestrial evidences. Glaciation started soon after this final warm peak. Although the data from Fjøsanger data cannot be strictly correlated with the marine cores, it suggests that a warming preceded inception over Scandinavia.

6. Summary and Conclusions

We present a physical mechanism for enhanced warmth in the eastern North Atlantic and along the path of the NwAC during times of minimum insolation forcing 115,000 years before present. Increased Arctic sea ice export in the East Greenland Current, as a direct result of the lower insolation, triggers nonlinear dynamical feedbacks of the subpolar gyre, and leads to a weaker circulation. This in turn increases the fraction of relatively warm and saline subtropical waters entering the Nordic Seas. The resulting increase in heat and salt transport into the Nordic Seas stabilizes ocean circulation and climate of the region. Comparison with marine sediment proxy data at the Fram Strait, Vøring Plateau and Rockall Plateau yields good agreement with the model results.

In addition to a warm eastern North Atlantic and Nordic Seas, the weaker subpolar gyre results in a northward shift of the North Atlantic Current, creating a warm anomaly in the central North Atlantic which can also be found in proxy data. This distinctive warming pattern is the fingerprint of a weaker subpolar gyre circulation at the last glacial inception. The combination of independent proxy data thus supports the dynamical hypothesis presented here.

Both marine and terrestrial proxy data indicate that large scale glacier growth started soon after the late Eemian warm phase [*Mangerud et al.*, 1981; *Risebrobakken et al.*, 2007], suggesting that the intrusion of Atlantic waters into the Nordic Seas played an important role for glacial inception over Scandinavia. Whether this warm water enhanced the air sea temperature contrast, increased moisture transport, and accelerated ice growth, or rather delayed ice growth due to warming is unclear.

Acknowledgments. We kindly acknowledge Pascale Braconnot for access to IPSL CM4 model output as well as discussions with Jan Mangerud, John Inge Svendsen and Tore Furevik. A.B. was funded by the Marie Curie Actions project NICE (MRTN-CT-2006-036127). Computer time was provided by the University of Bergen, Potsdam Institute for Climate Impact Research, Centre National de la Recherche Scientifique (IDRIS computing center) and the Commissariat à l'Energie Atomique (CCRT computing center). This is publication no. XXXX from the Bjerknes Centre for Climate Research.

References

Bauch, H. A., and H. Erlenkeuser (2008), A "critical" climatic evaluation of last interglacial (MIS 5e) records from the Norwegian Sea, *Polar Research*, *27*, 135–151.

Bauch, H. A., and E. S. Kandiano (2007), Evidence for early warming and cooling in North Atlantic surface waters during the last interglacial, *Paleoceanography*, *22*, PA1201.

Beckmann, A. (1998), *The representation of bottom boundary layer processes in numerical ocean circulation models. In: E.P. Chassignet and J. Verron, Editors: Ocean modeling and Parametrization*, pp. 135–154, Kluwer Academic Publishers, Dordrecht.

Berger, A. (1978), Long-Term Variations of Caloric Solar Radiation Resulting from the Earth's Orbital Elements, *Quaternary Research*, *9*, 139–167.

Born, A., and A. Levermann (2010), The 8.2k event: abrupt transition of the subpolar gyre towards a modern North Atlantic circulation, *Geochemistry, Geophysics, Geosystems*, *under review*.

Born, A., A. Levermann, and J. Mignot (2009), Sensitivity of the Atlantic ocean circulation to a hydraulic overflow parameterisation in a coarse resolution model: Response of the subpolar gyre, *Ocean Modelling*, *27 (3-4)*, 130–142.

Born, A., K. H. Nisancioglu, and P. Braconnot (2010), Sea ice induced changes in ocean circulation during the Eemian, *Climate Dynamics*, *online*, doi:10.1007/s00382-009-0709-2.

Braconnot, P., C. Marzin, L. Grégoire, E. Mosquet, and O. Marti (2008), Monsoon response to changes in Earth's orbital parameters: comparisons between simulations of the Eemian and of the Holocene, *Climate of the Past*, *4*, 281–294.

Calov, R., A. Ganopolski, V. Petoukhov, M. Claussen, V. Brovkin, and C. Kubatzki (2005), Transient simulation of the last glacial inception. Part II: sensitivity and feedback analysis, *Climate Dynamics*, *24*, 563–576.

Chapman, M. R., and N. J. Shackleton (1999), Global ice-volume fluctuations, North Atlantic ice-rafting events, and deep-ocean circulation changes between 130 and 70 ka, *Geology*, *27(9)*, 795–798.

Cortijo, E., S. Lehman, L. Keigwin, M. Chapman, D. Paillard, and L. Labeyrie (1999), Changes in meridional temperature and salinity gradients in the North Atlantic Ocean

(30°N-72°N) in the last interglacial period, *Paleoceanography*, *14(1)*, 23–33.

de Noblet, N., I. Prentice, S. Joussaume, D. Texier, A. Botta, and A. Haxeltine (1996), Possible Role of Atmosphere-Biosphere Interactions in Triggering the Last Glaciation, *Geophysical Research Letters*, *23*, 3191–3194.

Fichefet, T., and M. A. M. Maqueda (1997), Sensitivity of a global sea ice model to the treatment of ice thermodynamics and dynamics, *Journal of Geophysical Research*, *102*, 12,609.

Fichefet, T., and M. A. M. Maqueda (1999), Modelling the influence of snow accumulation and snow-ice formation on the seasonal cycle of the Antarctic sea-ice cover, *Climate Dynamics*, *15*, 251–268.

Gregory, J. M., et al. (2005), A model intercomparison of changes in the Atlantic thermohaline circulation in response to increasing atmospheric CO_2 concentration, *Geophysical Research Letters*, *32*, L12,703.

Hansen, B., and S. Østerhus (2000), North Atlantic - Nordic Seas exchanges, *Progress in Oceanography*, *45*, 109–208.

Hátún, H., A. B. Sandø, H. Drange, B. Hansen, and H. Valdimarsson (2005), Influence of the Atlantic Subpolar Gyre on the Thermohaline Circulation, *Science*, *309*, 1841–1844.

Hibler, W. D. (1979), A Dynamic Thermodynamic Sea Ice Model, *Journal of Physical Oceanography*, *9*, 815–846.

Hourdin, F., et al. (2006), The LMDZ4 general circulation model: climate performance and sensitivity to parametrized physics with emphasis on tropical convection, *Climate*

Dynamics, *27(7-8)*, 787–813.

Johannessen, T. (1987), Resente planktoniske foraminiferer fra Norskehavet, Islandhavet og Nordatlanteren: taksonomi, faunafordeling og stabil-isotopsammensetning, Master's thesis, Universitetet i Bergen, (Hovedoppgave til cand. scient. eksamen i marin geologi).

Kalnay, E., and coauthors (1996), The NCEP/NCAR 40-year reanalysis project, *Bull. Amer. Meteor. Soc.*, *77*, 437–471.

Khodri, M., Y. Leclainche, G. Ramstein, P. Braconnot, O. Marti, and E. Cortijo (2001), Simulating the amplification of orbital forcing by ocean feedbacks in the last glaciation, *Nature*, *410*, 570–574.

Krinner, G., N. Viovy, N. de Noblet-Ducoudre, J. Ogee, J. Polcher, P. Friedlingstein, P. Ciais, S. Sitch, and I. C. Prentice (2005), A Dynamic Global Vegetation Model for Studies of the Coupled Atmosphere - Biosphere System, *Global Biogeochemical Cycles*, *19(1)*, GB1015.

Levermann, A., and A. Born (2007), Bistability of the Atlantic subpolar gyre in a coarse-resolution model, *Geophysical Research Letters*, *34*, L24,605.

Levitus, S. (1982), *Climatological atlas of the world ocean. NOAA Professional Paper, vol 13*, 173 pp. pp., US Dept of Commerce, Washington DC.

Madec, G., P. Delecluse, M. Imbard, and C. Lévy (1997), *OPA version 8.1 Ocean General Circulation Model Reference Manual*, Institut Pierre-Simon Laplace, Note du Pôle de modélisation n^{o}11.

Mangerud, J., E. Sønstegaard, H.-P. Sejrup, and S. Haldorsen (1981), A continuous Eemian-Early Weichelian sequence containing pollen and marine fossils at Fjøsanger, western Norway, *Boreas*, *10*, 138–205.

Marti, O., et al. (2009), Key features of the IPSL ocean atmosphere model and its sensitivity to atmospheric resolution, *Climate Dynamics*, *34*, 1–26, doi:10.1007/s00382-009-0640-6.

McManus, J. F., D. W. Oppo, L. D. Keigwin, J. L. Cullen, and G. C. Bond (2002), Thermohaline Circulation and Prolonged Interglacial Warmth in the North Atlantic, *Quaternary Research*, *58*, 17–21.

Mignot, J., A. Levermann, and A. Griesel (2006), A decomposition of the Atlantic meridional overturning circulation into physical components using its sensitivity to vertical diffusivity., *Journal of Physical Oceanography*, *36*, 636–650.

Montoya, M., A. Griesel, A. Levermann, J. Mignot, M. Hofmann, A. Ganopolski, and S. Rahmstorf (2005), The Earth System Model of Intermediate Complexity CLIM*BER*-3α. Part I: description and performance for present-day conditions, *Climate Dynamics*, *25*, 237–263.

Montoya, M., A. Born, and A. Levermann (2010), Reversed North Atlantic gyre dynamics in glacial climate, *Climate Dynamics*, *online*, doi:10.1007/s00382-009-0729-y.

Petit, J. R., et al. (1999), Climate and atmospheric history of the past 420,000 years from the Vostok ice core, Antarctica, *Nature*, *399*, 429–436.

Petoukhov, V., A. Ganopolski, V. Brovkin, M. Claussen, A. Eliseev, C. Kubatzki, and S. Rahmstorf (2000), CLIM*BER*-2: a climate system model of intermediate complex-

ity. Part I: model description and performance for present climate, *Climate Dynamics*, *16*, 1.

Rasmussen, T. L., E. Balbon, E. Thomsen, L. Labeyrie, and T. C. E. van Weering (1999), Climate records and changes in deep outflow from the Norwegian Sea 150-55 ka, *Terra Nova*, *11(2/3)*, 61–66.

Risebrobakken, B., T. Dokken, and E. Jansen (2005), *The extent and variability of the Meridional Atlantic Circulation in the Nordic Seas during Marine Isotope Stage 5 and its influence on the inception of the last glacial. In: The Nordic Seas: An Integrated Perspective, edited by Drange, H., Dokken, T., Furevik, T., Gerdes, R., Berger, W. H.*, pp. 323–339, AGU Geophysical Monograph Series 158, Washington DC.

Risebrobakken, B., T. Dokken, O. H. Otterå, E. Jansen, Y. Gao, and H. Drange (2007), Inception of the Northern European ice sheet due to contrasting ocean and insolation forcing, *Quaternary Research*, *67*, 128–135.

Roberts, M. J., and R. A. Wood (1997), Topographic Sensitivity Studies with a Bryan Cox-Type Ocean Model, *Journal of Physical Oceanography*, *27*, 823–836.

Roullet, G., and G. Madec (2000), Salt conservation, free surface, and varying levels: A new formulation for ocean general circulation models, *Journal of Geophysical Research*, *105*, 23,927–23,942.

Ruddiman, W. F., and A. McIntyre (1975), Warmth of the Subpolar North Atlantic Ocean During Northern Hemisphere Ice-Sheet Growth, *Science*, *204*, 173–175.

Stouffer, R. J., et al. (2006), Investigating the Causes of the Response of the Thermohaline Circulation to Past and Future Climate Changes, *Journal of Climate*, *19*,

1365–1387.

Thorpe, R. B., R. A. Wood, and J. F. B. Mitchell (2004), Sensitivity of the modelled thermohaline circulation to the parameterisation of mixing across the Greenland-Scotland ridge, *Ocean Modelling*, *7*, 259–268.

Waelbroeck, C., L. Labeyrie, E. Michel, J. Duplessy, J. McManus, K. Lambeck, E. Balbon, and M. Labracherie (2002), Sea-level and deep water temperature changes derived from benthic foraminifera isotopic records, *Quaternary Science Reviews*, *21*, 295–305.

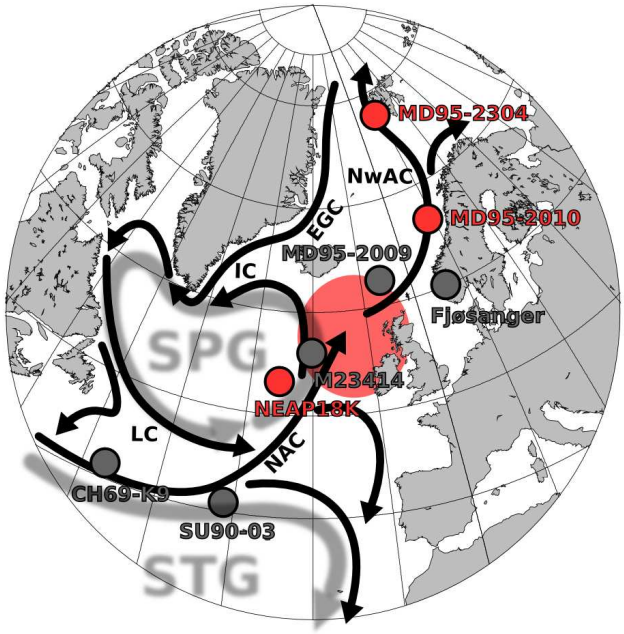

Figure 1. Map of the North Atlantic and Nordic Seas showing major ocean surface currents (arrows), marine sediment cores used in this study (red), and marine sediment cores and a terrestrial excavation site discussed in the text (gray). See Table 1 for references. Current systems of subpolar gyre (SPG) and subtropical gyre (STG) are illustrated in light gray. Source region of NwAC is highlighted in light red. Abbreviations: NAC, North Atlantic Current; NwAC, Norwegian Atlantic Current; EGC, East Greenland Current; LC, Labrador Current; IC, Irminger Current.

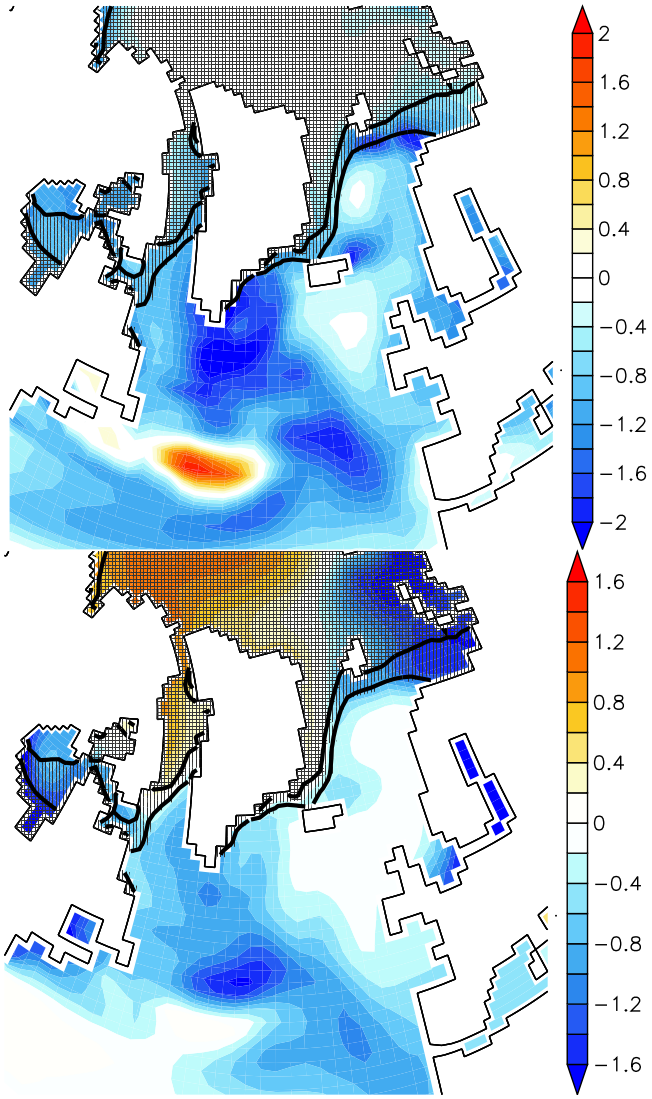

Figure 2. Differences 115k - 126k for IPSL CM4, averaged over the upper 50 m, **upper:** temperature in °C, **lower:** salinity in psu. Areas covered by more than 50 % sea ice annually averaged are hatched horizontally (126 ka) and vertically (115 ka) to mask regions directly affected by sea ice. Temperature and salinity show almost no change in the NwAC source region in the eastern North Atlantic and along the path of the Atlantic inflow into the Nordic Seas.

Table 1. Locations of marine sediment cores used or discussed in the text. Original references to previously published proxy records are given.

Core name	Position	Depth (m)	References
MD95-2304	78°N, 10°E	1315	*Risebrobakken et al.* [2005, 2007]
MD95-2010	67°N, 5°E	1226	*Risebrobakken et al.* [2005, 2007]
MD95-2009	63°N, 4°W	1027	*Rasmussen et al.* [1999]
Fjøsanger	60°N, 5°E	0	*Mangerud et al.* [1981]
M23414	54°N, 20°W	2196	*Bauch and Kandiano* [2007]
NEAP18K	52°N, 30°W	3275	*Chapman and Shackleton* [1999], *Cortijo et al.* [1999]
CH69-K9	41°N, 47°W	4100	*Cortijo et al.* [1999]
SU90-03	40°N, 32°W	2475	*Cortijo et al.* [1999]

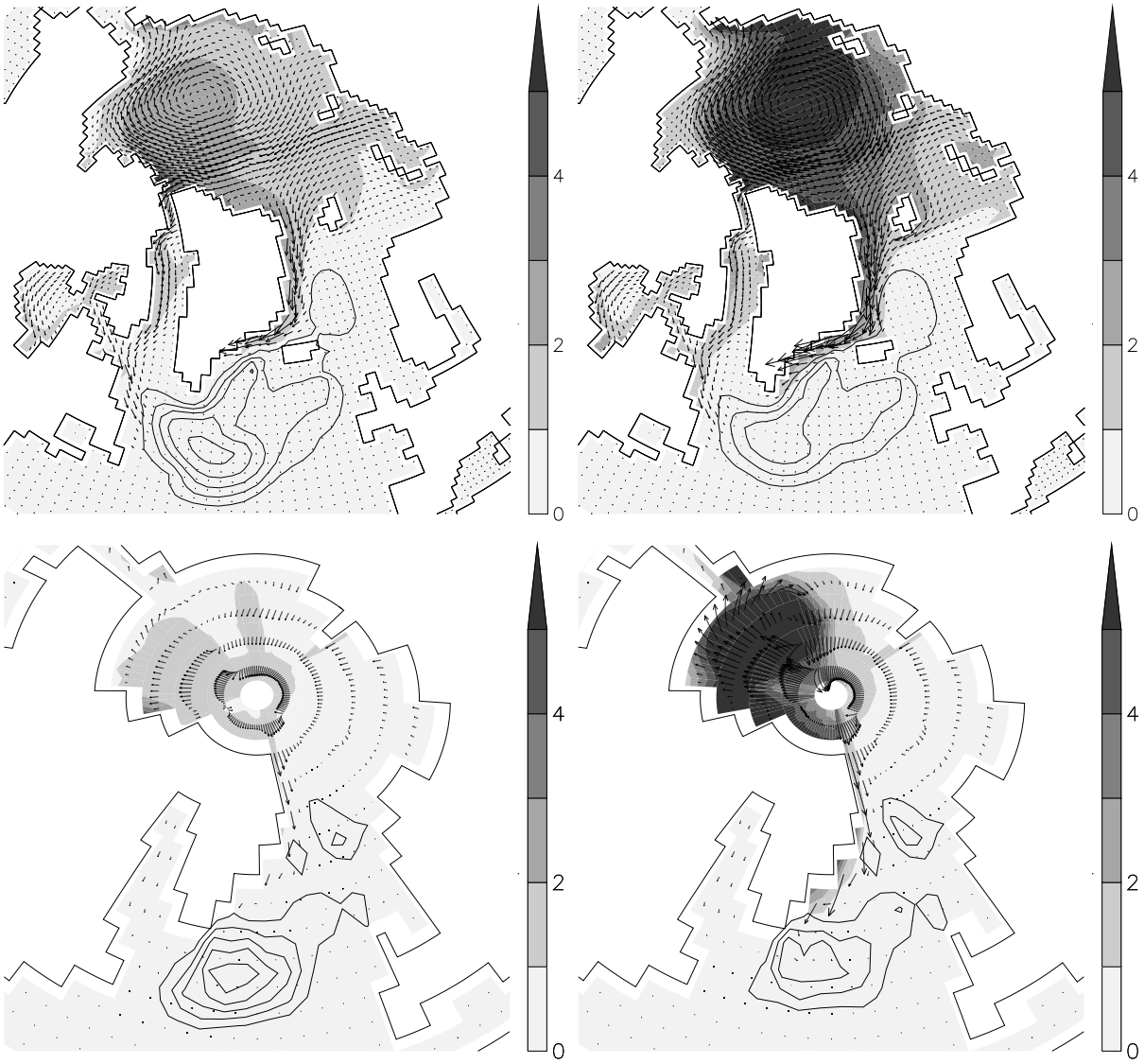

Figure 3. Sea ice thickness (shading, in m), sea ice volume transport (arrows, in m^2/s) and depth integrated stream function (contours, spacing 2 Sv, cyclonic flow only); **upper row:** IPSL CM4; **lower row:** CLIM*BER*-3α; **left column:** 126 ka; **right column:** 115 ka. Both models agree well on sea ice thickening in the Arctic Ocean, more sea ice export in the East Greenland Current and the consequential weakening of the subpolar gyre circulation.

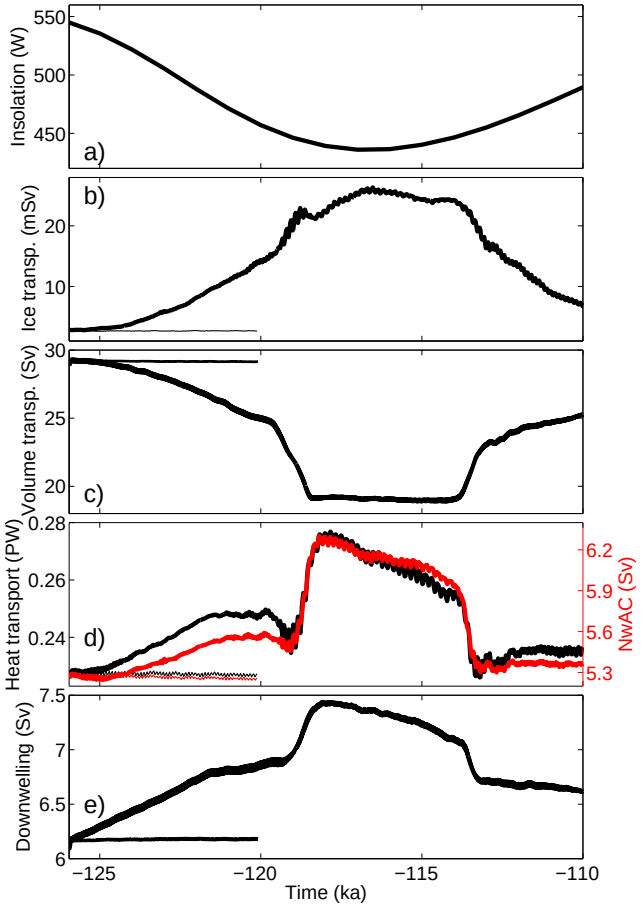

Figure 4. Key variables for climate evolution of the last glacial inception, averaged over 100 years. Thin lines show results of a 126 ka control experiment: **(a)** June insolation at 65°N; **(b)** southward sea ice transport through Denmark Strait; **(c)** circulation strength of the subpolar gyre; **(d)** heat transport (black) and volume transport (red) in the NwAC across a zonal section at 64°N; **(e)** downwelling in the Nordic Seas.

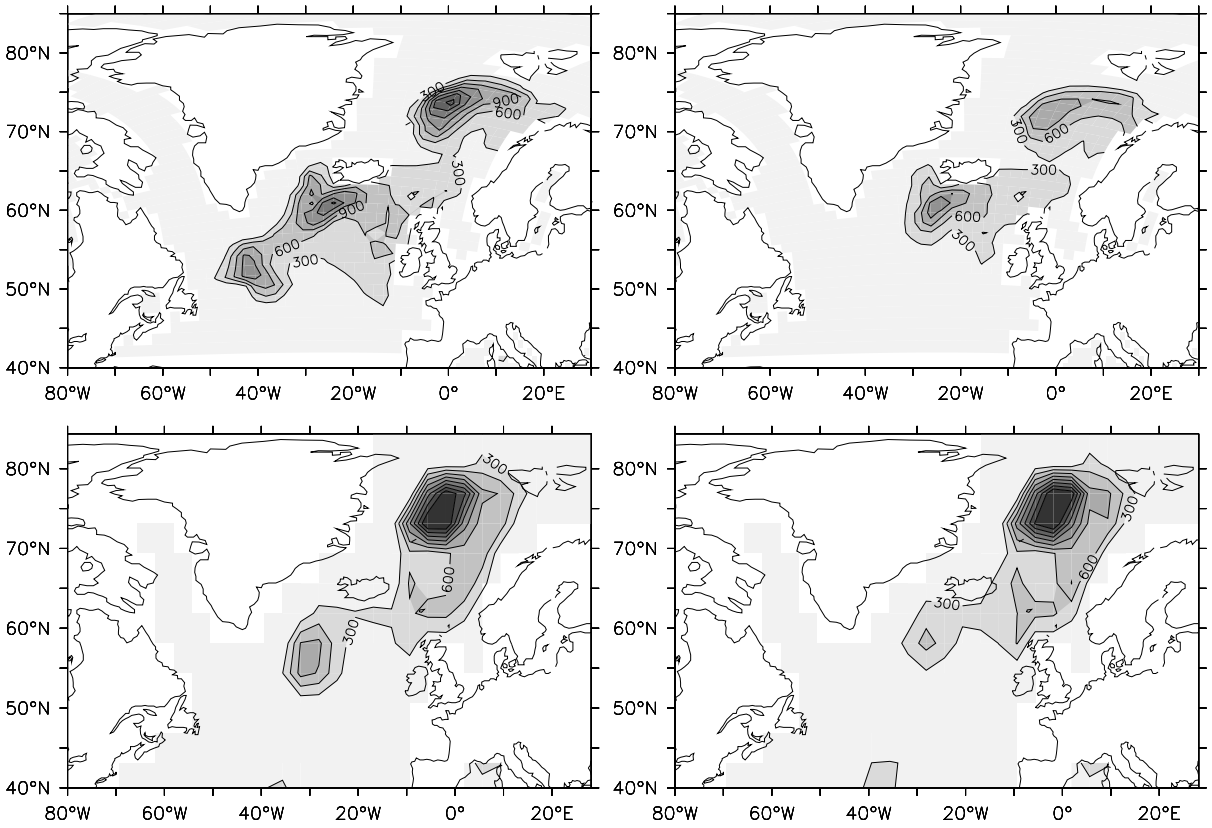

Figure 5. Mixed layer depth (in m); **upper row:** IPSL CM4; **lower row:** CLIM*BER*-3α; **left column:** 126 ka; **right column:** 115 ka. Deep convection in the Nordic Seas remains active at 115 ka in both models. South of the Greenland Scotland ridge, convection decreases leading to the shut-down of one convection region in IPSL CM4.

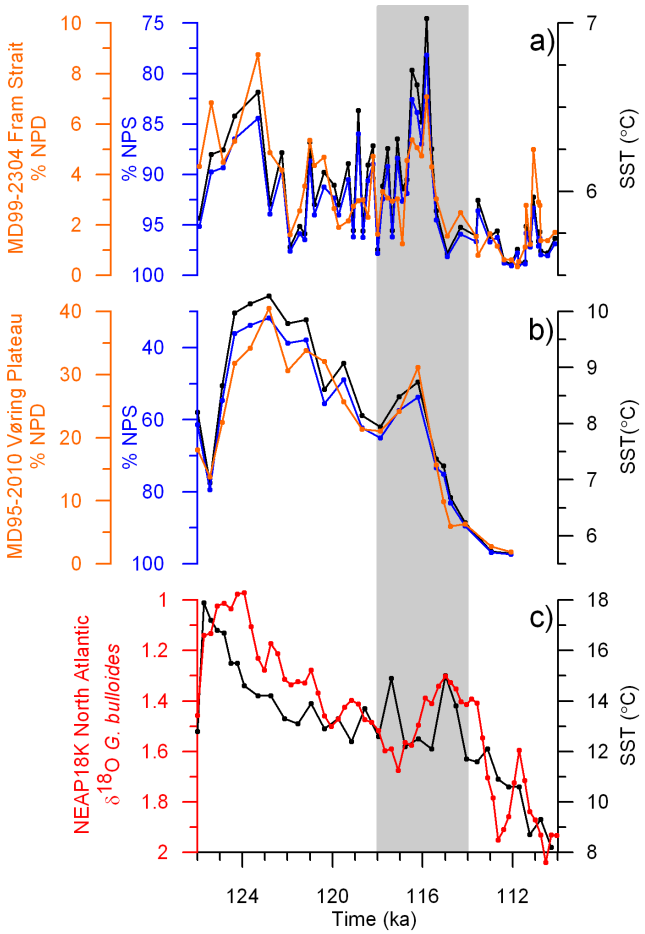

Figure 6. Proxy data reconstructions from the North Atlantic and Nordic Seas (see red dots in Fig. 1). Gray shading highlights period of maximum simulated heat transport in the NwAC (Fig. 4). **(a)** relative abundance of *N. pachyderma* (sin) (blue) and *N. pachyderma* (dex) (orange) at the western Spitsbergen slope (MD99-2304, *Risebrobakken et al.* [2007]). SST estimate based on the relative abundance of *N. pachyderma* (sin) is shown in black [*Johannessen*, 1987]; **(b)** Same as (a) but for the Vøring Plateau (MD95-2010); **(c)** *G. bulloides* $\delta^{18}O$ (red) (NEAP18K, *Chapman and Shackleton* [1999]) and SST estimate based on modern analog technique (black) [*Cortijo et al.*, 1999].